Acta Crystallographica Section B
Structural Science
ISSN 0108-7681

Octahedral tilting in Pb-based relaxor ferroelectrics at high pressure

Bernd J. Maier,[a]* Ross J. Angel,[b]* William G. Marshall,[c] Boriana Mihailova,[a] Carsten Paulmann,[a] Jens M. Engel,[d] Marin Gospodinov,[e] Anna-Maria Welsch,[a] Dimitrina Petrova[e,f] and Ulrich Bismayer[a]

[a]Department Geowissenschaften, Universität Hamburg, Grindelallee 48, 20146 Hamburg, Germany, [b]Crystallography Laboratory, Department of Geosciences, Virginia Tech, Blacksburg, VA 24060, USA, [c]ISIS Neutron Facility, STFC Rutherford Appleton Laboratory, Harwell Science and Innovation Campus, Chilton, Didcot, Oxon OX11 0QX, England, [d]Institut für Werkstoffwissenschaft, Technische Universität Dresden, Helmholtzstraße 7, 01069 Dresden, Germany, [e]Institute of Solid State Physics, Bulgarian Academy of Sciences, Blvd. Tzarigradsko Chausse 72, 1784 Sofia, Bulgaria, and [f]South-West University 'Neofit Rilski', 66 Ivan Mihailov str., 2700 Blagoevgrad, Bulgaria

Correspondence e-mail: bernd.maier@mineralogie.uni-hamburg.de, rangel@vt.edu

Received 6 November 2009
Accepted 21 April 2010

We have employed a combination of powder neutron diffraction and single-crystal synchrotron X-ray diffraction to characterize the pressure-induced phase transitions that occur in the perovskite-type relaxor ferroelectric $PbSc_{0.5}Ta_{0.5}O_3$ (PST) and $Pb_{0.78}Ba_{0.22}Sc_{0.5}Ta_{0.5}O_3$ (PST-Ba). At ambient pressure the symmetry of the average structure for both compounds is $Fm\bar{3}m$ as a result of partial ordering of the Sc and Ta cations on the octahedral sites. At pressures above the phase transition both the neutron and X-ray diffraction patterns exhibit an increase in the intensities of h,k,l = all odd reflections and no appearance of additional Bragg reflections. Synchrotron single-crystal X-ray diffraction data show that the intensity of hhh peaks, $h = 2n + 1$, does not change with pressure. This indicates that the structural distortion arising from the phase transition has a glide-plane pseudo-symmetry along the $\langle 111 \rangle$ cubic directions. Rietveld refinement to the neutron powder data shows that the high-pressure phase has either $R\bar{3}c$ or $R\bar{3}$ symmetry, depending on whether the presence of 1:1 octahedral cation ordering is neglected or taken into account, and comprises octahedral tilts of the type $a^-a^-a^-$ that continuously evolve with pressure. The cubic-to-rhombohedral transition is also marked by a large increase in the anisotropy of the displacement ellipsoids of the Pb cations, indicating larger displacements of Pb cations along the rhombohedral threefold axis rather than within the perpendicular plane. For PST the anisotropy of the Pb displacement parameters decreases at approximately 3 GPa above the phase-transition pressure. For both PST and PST-Ba the average magnitudes of Pb-cation displacements expressed in terms of isotropic displacement ellipsoids gradually decrease over the entire pressure range from ambient to 7.35 GPa.

1. Introduction

Relaxor ferroelectrics are of great technological importance for a wide range of applications, including memory devices (Bhalla *et al.*, 2000; Gruverman & Kholkin, 2006). They exhibit outstanding dielectric, electroelastic and electro-optic properties due to their complex nanoscale structure (Bokov & Ye, 2006; Hirota *et al.*, 2006), consisting of polar nanoregions (PNRs) dispersed in a paraelectric matrix (Bursill *et al.*, 1995). In the vicinity of the temperature of the dielectric permittivity maximum T_m at room pressure PNRs create and annihilate on a microsecond timescale (Blinc *et al.*, 2000) and vary in size and shape (Bursill *et al.*, 1995), resulting in a broad frequency-dependent peak of the dielectric permittivity *versus* temperature (Bokov & Ye, 2006; Samara, 2003). PNRs nucleate at temperatures well above T_m and for canonical relaxors they do not develop into normal ferroelectric domains at temperatures below T_m (Bokov & Ye, 2006). The

majority of relaxors have an ABO_3 perovskite-type structure (Fig. 1) with Pb cations on the A site and two types of cations on the B site that may become ordered by alternating along the ⟨100⟩ directions. In the case of the absence of long-range 1:1 chemical B-site order, the average structure has a primitive cubic symmetry ($Pm\bar{3}m$) with a unit-cell parameter of $a_0 \simeq 4$ Å. If the B-site cations are chemically ordered, the unit cell is doubled, with a unit-cell parameter equal to $2a_0 \simeq 8$ Å and the symmetry of the average structure is face-centred cubic ($Fm\bar{3}m$).

The atomistic mechanism of suppression of long-range ferroelectric order is still not well understood. The underlying concept of most of the theoretical models is that the B-site chemical disorder and related local charge imbalance are the major factors for the occurrence of relaxor behaviour (Kleemann *et al.*, 1998; Samara, 2003; Burton *et al.*, 2005). However, synchrotron X-ray diffraction (XRD) and transmission electron microscopy provide some evidence that the coexistence of competing ferroelectric and antiferroelectric coupling may also play a key role in the formation of the relaxor state (Baba-Kishi *et al.*, 1992; Takesue *et al.*, 1999; Tkachuk & Chen, 2003).

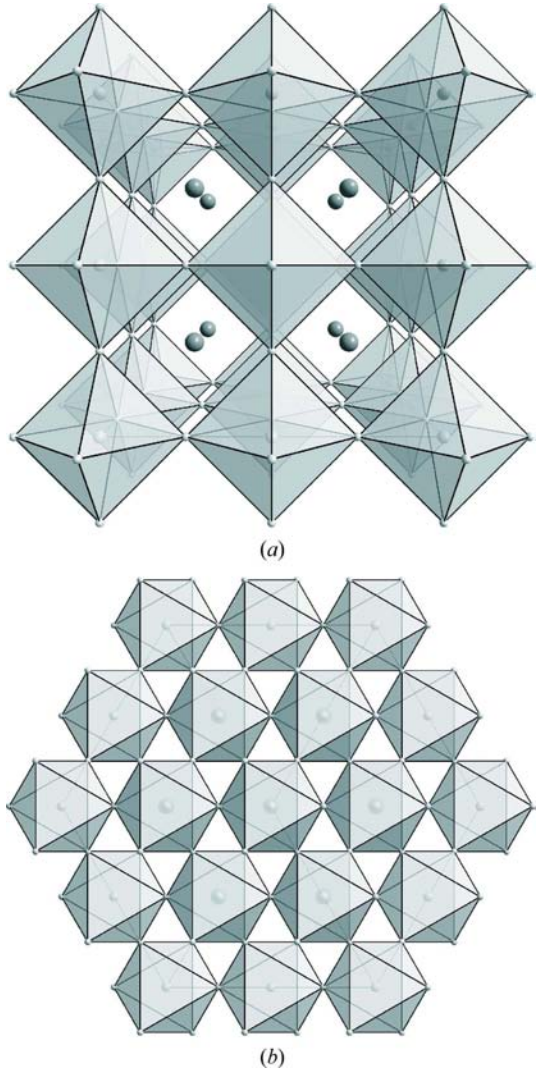

Figure 1
The ideal perovskite-type structure in a perspective view along the cubic ⟨100⟩ direction (*a*) and in a plane view along the cubic ⟨111⟩ direction (*b*).

Pressure can help to resolve the structural complexities of relaxors because external elastic forces can slow down dynamic structural fluctuations and thus better reveal the intrinsic structural features. Recently, it was shown that the diffuse X-ray scattering arising from PNRs is gradually suppressed with increasing pressure (Chaabane *et al.*, 2003; Kreisel *et al.*, 2003; Ahart *et al.*, 2005; Janolin *et al.*, 2006; Mihailova, Angel *et al.*, 2008). The high-pressure Raman scattering of Pb-based relaxors is inconsistent with the paraelectric cubic symmetry but it also differs from the Raman scattering observed at low temperatures (Kreisel *et al.*, 2002; Chaabane *et al.*, 2004; Ahart *et al.*, 2005; Janolin *et al.*, 2006; Mihailova, Angel *et al.*, 2008; Welsch, Mihailova *et al.*, 2009). These experimental findings indicate that pressure rearranges the ferroic atomic displacements existing at ambient conditions and favours long-range ordering processes comprising structural species which are not enhanced on cooling.

Synchrotron single-crystal XRD on $PbMg_{1/3}Nb_{2/3}O_3$ (PMN) showed that pressure induces weak superlattice Bragg reflections of the type h,k,l all odd, indexed in $Fm\bar{3}m$ (Chaabane *et al.*, 2003). Additionally, Chaabane *et al.* (2003) reported that, according to their own unpublished data on PMN, these superlattice reflections also appear in the high-pressure neutron diffraction patterns, but with very weak intensities. The authors concluded that pressure induces ordered anti-parallel cation displacements, thus leading to a doubling of the unit cell. In a subsequent paper on high-pressure synchrotron XRD and Raman scattering from $PbZn_{1/3}Nb_{2/3}O_3$ (PZN), Janolin *et al.* (2006) interpreted the continuous increase in X-ray superlattice peaks with increasing pressure as indicative of the development of a rhombohedral pattern of octahedral tilts. This would be consistent with the general principle that '2:4' perovskites with an average cation charge of 4+ on the octahedral sites undergo tilt transitions to lower-symmetry structures with greater tilts on increasing pressure (Angel *et al.*, 2005). On the other hand, pressure-induced superlattice Bragg reflections were not detected by powder neutron diffraction data on $PbMg_{1/3}Ta_{2/3}O_3$ (PMT; Gvasaliya *et al.*, 2006) and PMN (Rotaru *et al.*, 2008) which would be a surprising result in the presence of octahedral tilting, as the superlattice peak intensities would be dominated by scattering from the O atoms. However, the refinements of Gvasaliya *et al.* (2006) on PMT and Rotaru *et al.* (2008) on PMN show that the magnitudes of the Pb displacements decrease with pressure, while the anisotropy of the oxygen displacements within a cubic average structure increases in a way consistent with the development of octahedral tilting.

Among the known Pb-based relaxors, $PbSc_{0.5}Ta_{0.5}O_3$ (PST) is a very suitable model compound to study pressure-induced structural changes in this class of materials because at room temperature and ambient pressure PST is in the ergodic state, close to T_m, and exhibits an abundance of PNRs (Mihailova, Maier *et al.*, 2008). In addition, the stoichiometry of this

Table 1
Load, pressure and integrated proton current (IPC) at the ISIS target for the neutron powder diffraction patterns.

PST			PST-Ba		
Load (tns)	*P* (GPa)	IPC (μAh)	Load (tns)	*P* (GPa)	IPC (μAh)
0	0.00 (0)	175	0	0.00 (0)	95
6	0.13 (3)	443	6	0.00 (3)	170
9	0.40 (4)	110	10	0.17 (3)	112
13	1.09 (2)	1046	14	0.59 (4)	103
17	1.51 (2)	1046	17.5	0.98 (2)	904
20	1.84 (3)	986	30	2.54 (4)	170
25	2.63 (3)	1046	35	3.52 (3)	691
34	3.58 (3)	1046	65	6.87 (4)	871
54	5.10 (4)	1155			
64	5.48 (5)	345			
75	7.35 (4)	2214			

compound allows for the existence of spatial regions with a chemical 1:1 B-site long-range order embedded in a chemically disordered matrix. Recently, it has been shown that PST undergoes a continuous phase transition near 1.9 GPa (Mihailova, Angel *et al.*, 2008), which is detectable by high-resolution single-crystal XRD. The combined synchrotron single-crystal XRD and Raman scattering data provide strong evidence that the high-pressure phase is rhombohedral and that it involves coherent distortion of the Pb environment, consistent with anti-phase BO_6 tilting (Mihailova, Angel *et al.*, 2008). *A*-site doping of PST with Ba suppresses the formation of long-range ferroelectric ordering at low temperatures, regardless of the sample having nearly the same degree of 1:1 *B*-site chemical order and larger mean size of *B*-site chemically ordered regions as compared to pure PST (Marinova *et al.*, 2006; Mihailova, Angel *et al.*, 2008). Besides, the dilution of the Pb system with Ba smears out the pressure-induced phase transition over a considerable pressure range (Welsch, Maier *et al.*, 2009). The Ba-induced renormalization of both temperature- and pressure-driven structural transformations is due to the formation of local elastic fields in the vicinity of incorporated Ba cations.

Structural refinements and symmetry analyses based only on XRD data are restricted by the weak scattering of the O atoms compared with the cations, and very significant absorption and extinction issues. Therefore, in order to completely determine the high-pressure structural state of Pb-based relaxors, we performed a study of PST and PST-Ba with both powder neutron diffraction and synchrotron single-crystal X-ray diffraction.

2. Experimental methods

Cubic shaped, partially *B*-site ordered single crystals of PST and $Pb_{0.77}Ba_{0.23}Sc_{0.5}Ta_{0.5}O_3$ (PST-Ba) were synthesized by the high-temperature solution growth method (Marinova *et al.*, 1997, 2006).

High-pressure time-of-flight neutron powder diffraction was performed with powders made from the same single crystals of PST and PST-Ba using a Paris–Edinburgh (PE) pressure cell (Besson *et al.*, 1992; Nelmes *et al.*, 1994; Marshall & Francis, 2002) at PEARL, ISIS/RAL (ISIS Annual Report, 1996, 1997), using a perdeuterated 4:1 methanol–ethanol mixture as the pressure medium to ensure hydrostatic conditions. Pressure was determined using the equations-of-state of the samples previously determined by in-house single-crystal XRD measurements (Mihailova, Angel *et al.*, 2008; Welsch, Maier *et al.*, 2009). Neutron powder patterns were collected at several pressures for the exposure times listed in Table 1. Both samples were measured after decompression at $p = 0$ to verify the reversibility of the structural changes occurring upon pressurization. Structure refinements were carried out using EXPGUI/GSAS (Toby, 2001; Larson & Von Dreele, 1994), using the *GSAS* time-of-flight profile peak shape consisting of a convolution of two back-to-back exponentials and a pseudo-Voigt function. The background was fitted using a 12-term cosine Fourier series.

High-pressure synchrotron single-crystal XRD experiments were conducted on the beamline F1 at HASYLAB/DESY, using a MarCCD 165 detector. An incident radiation of wavelength $\lambda = 0.5000$ and 0.4500 Å and a sample-to-detector distance of 100 and 80 mm were used for PST and PST-Ba. The experiments were performed with a plate diamond–anvil cell (DAC) of Boehler–Almax design (Boehler, 2006) and a 4:1 methanol–ethanol mixture to ensure hydrostatic conditions up to 9.8 GPa (Angel *et al.*, 2007). The ruby-line luminescence method was used to determine pressure (Munro *et al.*, 1985). For both compounds data were collected on {100} cuts of approximate size $\sim 100 \times 100 \times 50\ \mu m^3$ with a stepwidth of 0.5° per frame and an exposure time of 120 s. Additionally, short-time (1 and 5 s) data collections were performed on PST to correctly quantify the integrated intensities. A {110}-cut PST crystal was also measured in order to gain access to reflections of the type *hhh* with $h = 2n + 1$, which helped to clarify the symmetry changes. The collected data were scaled with the primary beam intensity using SCLMAR (Paulmann & Malcherek, 2006) in order to compensate for the synchrotron beam decay. The scaled data were subsequently integrated with the Oxford Diffraction software *CrysAlis*™ (Oxford Diffraction, 2007). Structure models were refined to the integrated intensities of PST using *SHELX* (Sheldrick, 2008).

3. Results

3.1. Low-pressure phase

At room pressure and temperature PST and PST-Ba exhibit a metrically cubic structure consisting of a paraelectric perovskite-type matrix in which PNRs are dispersed. According to XRD, both compounds exhibit partial *B*-site chemical order and their average structure therefore has $Fm\bar{3}m$ symmetry. In this symmetry, Bragg reflections whose indices have *h*,*k*,*l* all even (eee reflections) arise from the primitive-cubic perovskite-type structure, whereas Bragg reflections with *h*,*k*,*l* all odd (ooo reflections) arise solely from *B*-site 1:1 chemically ordered regions and reflect the average long-range chemical *B*-site cation order within the sample.

Table 2
Unit-cell parameters of PST in hexagonal and cubic settings obtained from refinements to neutron powder diffraction data.

For all pressures a model with disordered *B*-site cation sites was refined. The doubling of the pseudo-cubic unit cell at pressures above 1.09 GPa results from the occurrence of anti-phase octahedral tilts.

P (GPa)	Space group	*a* (Å)	*c* (Å)	a_{cub}	α_{cub} (°)	χ^2_w
0.00 (0)	$Pm\bar{3}m$	–	–	4.0826 (3)	90.00 (0)	1.298
0.13 (3)	$Pm\bar{3}m$	–	–	4.0811 (2)	90.00 (0)	1.597
0.40 (4)	$Pm\bar{3}m$	–	–	4.0773 (3)	90.00 (0)	1.216
1.09 (2)	$R\bar{3}c$	5.7541 (8)	14.091 (4)	8.1368 (16)	90.01 (2)	1.982
1.51 (2)	$R\bar{3}c$	5.7444 (9)	14.078 (4)	8.1251 (17)	89.98 (2)	2.114
1.84 (3)	$R\bar{3}c$	5.7373 (9)	14.056 (4)	8.1143 (17)	89.99 (2)	1.998
2.63 (3)	$R\bar{3}c$	5.7264 (8)	14.029 (3)	8.0988 (11)	90.00 (2)	2.002
3.58 (3)	$R\bar{3}c$	5.7147 (5)	13.996 (3)	8.0814 (11)	90.01 (2)	2.135
5.10 (4)	$R\bar{3}c$	5.7002 (5)	13.935 (2)	8.0560 (9)	90.08 (2)	2.041
5.48 (5)	$R\bar{3}c$	5.7001 (6)	13.901 (2)	8.0493 (10)	90.17 (2)	1.325
7.35 (4)	$R\bar{3}c$	5.6828 (4)	13.844 (2)	8.0221 (6)	90.21 (2)	2.585

Table 3
Unit-cell parameters of PST-Ba in hexagonal and cubic settings obtained from refinements to neutron powder diffraction data.

For all pressures a model with disordered *B*-site cation sites was refined. The doubling of the pseudo-cubic unit cell at pressures above 3.52 GPa results from the development of anti-phase octahedral tilts.

P (GPa)	Space group	*a* (Å)	*c* (Å)	a_{cub}	α_{cub} (°)	χ^2_w
0.00 (0)	$Pm\bar{3}m$	–	–	4.0837 (1)	90.00 (0)	1.352
0.17 (3)	$Pm\bar{3}m$	–	–	4.0812 (1)	90.00 (0)	1.218
0.59 (4)	$Pm\bar{3}m$	–	–	4.0762 (1)	90.00 (0)	1.189
0.98 (2)	$Pm\bar{3}m$	–	–	4.0717 (1)	90.00 (0)	2.134
2.75 (4)	$Pm\bar{3}m$	–	–	4.0529 (1)	90.00 (0)	1.281
3.52 (3)	$R\bar{3}c$	5.7373 (9)	14.056 (4)	8.0922 (11)	89.99 (2)	1.910
6.87 (4)	$R\bar{3}c$	5.6796 (5)	13.919 (3)	8.0356 (12)	89.98 (2)	1.821

The XRD ooo reflections are weak for both PST and PST-Ba, revealing a low degree of *B*-site order. However, peak-width analysis of high-resolution powder XRD showed that PST-Ba has larger *B*-site ordered domains (33 nm) compared with PST (6 nm; Mihailova, Maier *et al.*, 2008). Structure refinements in $Fm\bar{3}m$ to the low-pressure synchrotron single-crystal XRD data also reveal a smaller *B*-site cation order parameter for PST {Q_{od} = |SOF(Ta) − SOF(Sc)|/[SOF(Ta) + SOF(Sc)] = 0.08 (2) at 0.5 GPa} than for PST-Ba [Q_{od} = 0.23 (2) at ambient pressure; Marinova *et al.*, 2006].

Synchrotron single-crystal XRD data on both compounds show strong diffuse scattering streaks along the ⟨110⟩* direction which indicate the existence of abundant PNRs at ambient conditions. The diffuse scattering is strongly suppressed above the critical pressure of 1.9 GPa for PST (Mihailova, Angel *et al.*, 2008) and above 4 GPa for PST-Ba (Welsch, Maier *et al.*, 2009). Diffuse scattering around eee reflections was not observable in the neutron powder diffraction patterns at any pressure. Nor were the ooo reflections detected by neutron powder diffraction up to 1.09 (2) GPa for PST and up to 3.52 (3) GPa for PST-Ba (Fig. 2). The absence of the ooo reflections can be attributed to the low degree of *B*-site cation order and the considerably lower scattering contrast of Sc and Ta for neutrons compared with X-rays. It is therefore not possible to determine the state of the *B*-site cation order from the neutron powder data, and consequently the state of chemical cation order on the *B* sites does not affect the refined values of the model parameters in the $Fm\bar{3}m$ structure. The O-atom position is also fixed at $00\frac{1}{4}$ by the absence of ooo-reflection intensity. Rietveld refinements to low-pressure neutron diffraction datasets revealed that the O atom displays significant anisotropy in the atomic displacement parameters. At ambient pressure U^{11} and U^{33} are equal to 0.033 (1) and 0.013 (1) Å^2 for PST and to 0.0242 (8) and 0.010 (1) Å^2 for PST-Ba; for both compounds $U^{11} = U^{22} \simeq 2.5U^{33}$. This may be indicative of static and/or dynamic local octahedral tilting within the structure, similar to that observed close to tilt transitions in other perovskites (*e.g.* Goodwin *et al.*, 2007). It is worth noting that the structure refinement to the 0.5 GPa synchrotron XRD data of PST in $Fm\bar{3}m$ also yields the same pattern of anisotropy in the O-atom displacement parameters. This anisotropy slightly increases with pressure when approaching the high-pressure regime in which the structure is better refined in non-cubic settings.

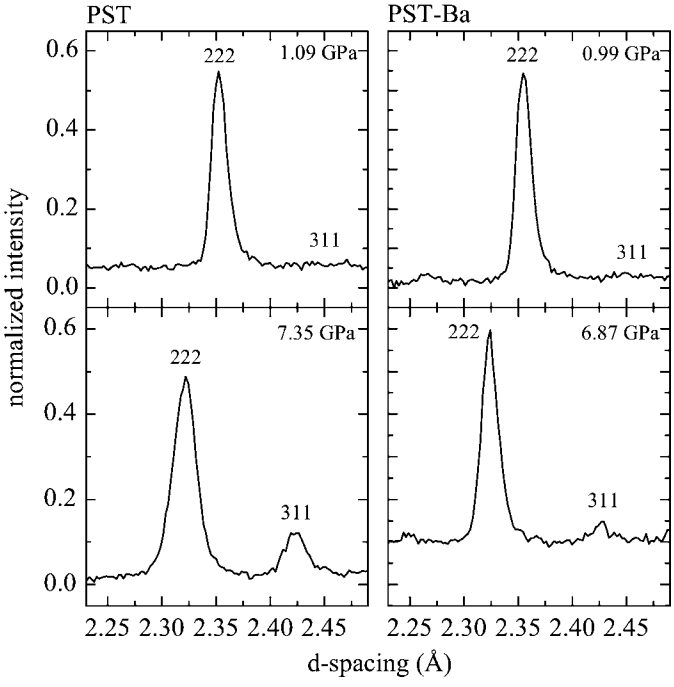

Figure 2
Sections of the neutron powder diffraction patterns at low and high pressures for PST and PST-Ba. Indices are given in $Fm\bar{3}m$.

For both PST and PST-Ba, the isotropic displacement parameter of the *B*-site cation obtained by the refinement to the ambient-pressure neutron powder diffraction patterns is 0.007 (1) Å^2, while that of the Pb cation on the *A* site is 0.049 (1) Å^2. The relatively large isotropic displacement parameter of Pb indicates incoherent static and/or dynamic off-centre Pb displacements with a mean value slightly greater than 0.2 Å, which is consistent with the Pb off-centred shifts in lead-based relaxors estimated by other methods (Peng & Bursill, 1993; Zhou *et al.*, 2004). The isotropic displacement

parameters of *B* cations do not change with pressure within their uncertainties, while those of Pb cations gradually decrease with increasing pressure. Free refinements of a split position for the Pb site in the manner of Gvasaliya *et al.* (2006) resulted in the Pb refining to the special position at $\frac{1}{4}\frac{1}{4}\frac{1}{4}$ within the uncertainties. The refined unit-cell parameters are given in Tables 2 and 3 for PST and PST-Ba, respectively.

3.2. High-pressure phase: PST

At pressures above 1.51 (2) GPa the neutron powder diffraction patterns exhibit ooo reflections that are as sharp as the main eee reflections (Fig. 2). They significantly increase in intensity with increasing pressure (see Fig. 3). In general, three possible structural features could contribute to the intensity of these pressure-induced ooo reflections: chemical 1:1 *B*-site cation ordering, ordering of Pb and/or *B*-cation off-centred displacements in a pattern that maintains an *F* lattice, and octahedral tilting. As discussed above, the only contribution at low pressures to the intensities of the ooo reflections is from the *B*-site ordering. Given that the experiments are performed at room temperature, it is very unlikely that any changes in the *B*-site cation distribution could occur upon pressurization and, hence, the pressure-enhancement of ooo reflections cannot result from an increase in the degree of chemical *B*-cation order. The isotropy and the very small values of the atomic displacement parameters of *B* cations for all the pressure points studied indicate that within the sensitivity of diffraction the *B* cations are not off-centred and, therefore, ordering of off-centre displacements of *B* cations is implausible. Raman scattering data also show that pressure suppresses the local off-centring of *B* cations (Mihailova, Angel *et al.*, 2008; Welsch, Maier *et al.*, 2009).

Fig. 4 shows the $h\bar{1}\bar{1}$ line in reciprocal space of a {110}-cut PST crystal at 4.2 GPa. With the exception of the 111 reflection that consists only of the weak and broad contribution from the *B*-site cation ordering, the intensities of the ooo reflections have significantly increased with pressure. Similarly, the systematic absence of reflections of the type *hhh*, $h = 2n + 1$, has been observed in disordered $PbSc_{0.5}Nb_{0.5}O_3$ (Maier *et al.*, 2010). This clearly indicates that the structural distortion developing at higher pressures exhibits a strong pseudo-glide symmetry along the cubic ⟨111⟩ directions which is only broken by the weak reflections arising from *B*-site cation ordering. The existence of a glide pseudo-symmetry is also consistent with ordering of the off-centred displacements of Pb cations. However, such long-range ordered shifts of Pb cations can only contribute to reflections with $l = 2n$, indexed in $Fm\bar{3}m$ and cannot be responsible for the increasing intensity of the $l = 2n + 1$ reflections in the high-pressure phase. Therefore, pressure-induced long-range order of tilted BO_6 octahedra is the only possible explanation for the increase in the intensities of ooo reflections, so we will further analyze in detail the possible tilt configurations in a perovskite-type structure built up of rigid octahedra. Note that there is also weak diffuse streaking along the ⟨100⟩* direction (Fig. 4) centred around the ooo Bragg reflections in the X-ray diffraction patterns. This streaking indicates that the octahedral tilting pattern is not completely homogeneous across the entire single-crystal sample.

Neither the neutron diffraction patterns, nor long-exposure (120 s) single-crystal synchrotron XRD patterns show evidence of any other additional diffraction maxima at high pressures. This means that only static distortions associated with phonon condensation at the *R* point of the Brillouin zone of the average $Pm\bar{3}m$ structure are involved in the high-pressure phase (Howard & Stokes, 2005). This mode corre-

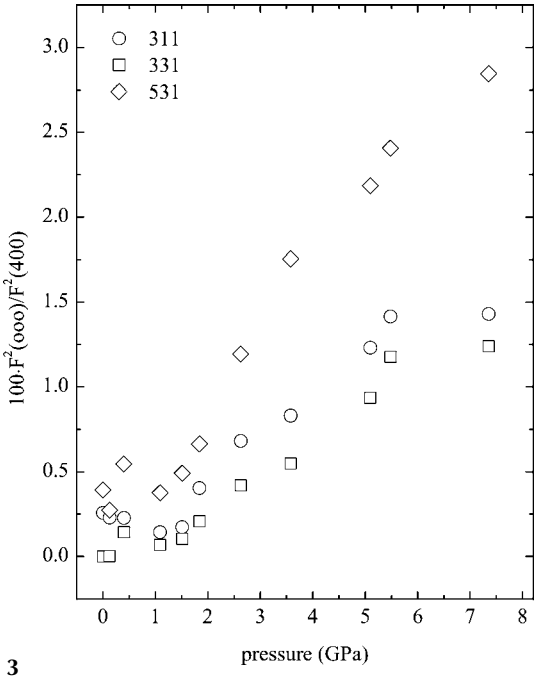

Figure 3
Pressure dependence of the normalized squared structure factor F^2_{hkl}/F^2_{400} for the superlattice reflections 311, 331 and 531 (indexed as $Fm\bar{3}m$) of PST obtained by LeBail fits to the neutron powder diffraction data.

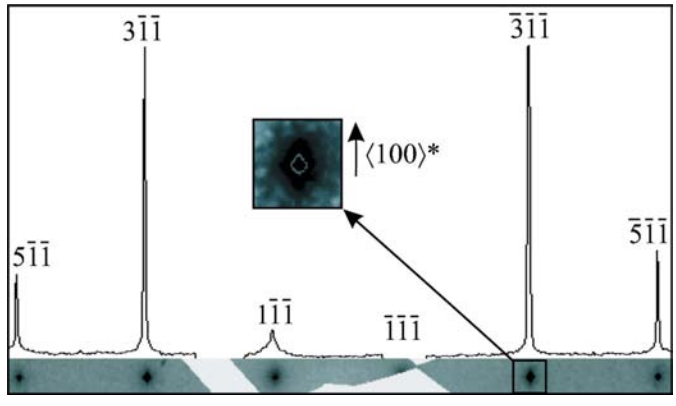

Figure 4
The $h\bar{1}\bar{1}$ line in reciprocal space at 4.2 GPa of a {110}-cut single crystal of PST, with the intensity profile along the line shown above. The visible $1\bar{1}\bar{1}$ reflection arises from chemical ordered domains only, therefore it appears broad and with weak intensity. The other reflections exhibit strong and sharp components arising from the octahedral tilting on top of the broad reflections originating from the chemically 1:1 *B*-site ordered domains.

sponds to anti-phase tilts of the octahedra about one or more of the unit-cell axes of the cubic structure. There are thus six possible symmetrically distinct octahedral tilt systems for the high-pressure phase, of which the three with the highest symmetry are $a^-a^-a^-$, $a^0b^-b^-$ and $a^0a^0c^-$ in Glazer notation (Glazer, 1972). The remaining three, $a^-b^-c^-$, $a^-b^-b^-$ and $a^0b^-c^-$, are sub-groups of these (Howard & Stokes, 2005). We will only consider the three highest-symmetry tilt systems as the resolution of the neutron powder diffraction data does not allow us to reliably refine the more complex lower-symmetry structures that correspond to *B*-site chemically disordered systems. In a perovskite with completely disordered cations on the *B* sites the corresponding space-group symmetries are $R\bar{3}c$ ($a^-a^-a^-$), *Imma* ($a^0b^-b^-$) and $I4/mcm$ ($a^0a^0c^-$). The same configurations of tilts can develop from the aristotype structure of a chemically *B*-site ordered system with $Fm\bar{3}m$ symmetry, and the corresponding space groups for the three highest-symmetry tilts are $R\bar{3}$ ($a^-a^-a^-$), $C2/m$ ($a^0b^-b^-$) and $I4/m$ ($a^0a^0c^-$), see Howard *et al.* (2003). Thus, anti-phase octahedral tilting can be developed throughout the sample bulk, regardless of the intrinsic chemical inhomogeneity of $(Pb,A'')(B',B'')O_3$ relaxors.

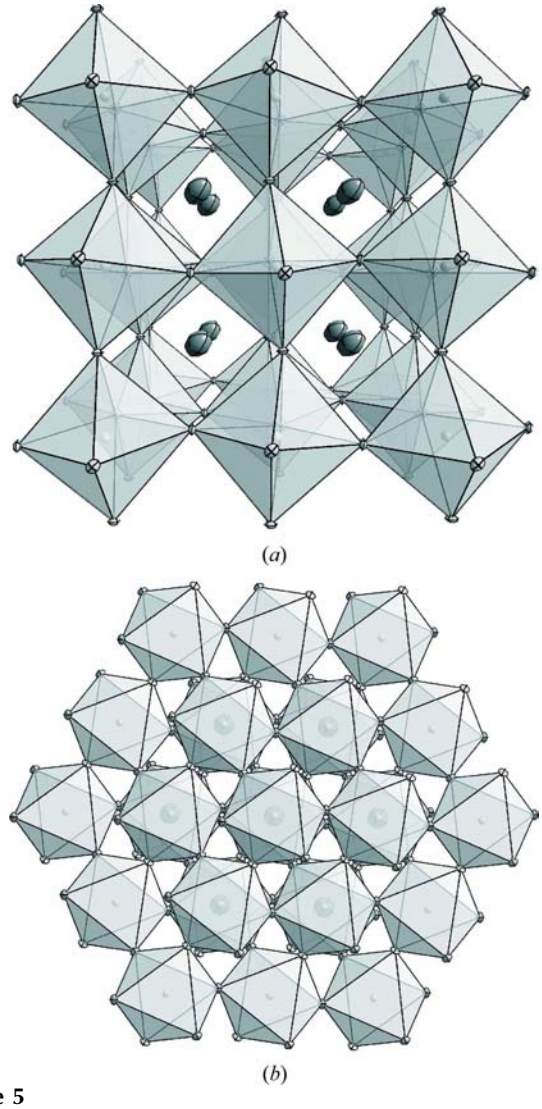

Figure 5
The time- and space-averaged high-pressure structure of PST at 7.35 GPa in $R\bar{3}c$ in a perspective view along the pseudo-cubic ⟨100⟩ direction (*a*) and in a plane view along the pseudo-cubic ⟨111⟩ direction (*b*). The bright ellipsoids denote O atoms with anisotropic atomic displacement parameters which form octahedra around the *B* cations with an $a^-a^-a^-$ tilt pattern. The dark ellipsoids represent Pb cations, having anisotropic atomic displacements enhanced along the pseudo-cubic ⟨111⟩ direction.

3.2.1. Rhombohedral systems. Due to the *c*-glide pseudo-symmetry of the structural distortion at high pressures and the weak contribution of the *B*-site cation ordering to the intensities of the ooo reflections in neutron powder diffraction, initial refinements were performed with a *B*-site disordered model in the space group $R\bar{3}c$. Rietveld refinements to the data were completed with isotropic displacement parameters for the *B* site, as anisotropic refinement resulted in isotropic values, and anisotropic displacement parameters for the Pb and O sites. The refined high-pressure structure of PST exhibits strong octahedral tilting and significantly anisotropic displacements of the Pb cations (see Fig. 5).

The α angle of the pseudo-cubic unit cell measures the symmetry-breaking strain from the cubic phase. However, due to the limited resolution of the diffractometer the measured neutron powder patterns cannot resolve the small distortion from cubic existing above 1.9 GPa (Mihailova, Angel *et al.*, 2008), resulting in a correlation of the lattice parameters of the high-pressure phase with the peak-width parameters. Thus, the refined value of the pseudo-cubic α angle is not a reliable estimate of the distortion of the structure from cubic symmetry. Therefore, we used the octahedral tilt angle $\omega(p)$ determined from the structure refinements as a more reliable measure for the distortion, as it is derived mainly from the intensities of the ooo reflections. In $R\bar{3}c$ perovskites, the octahedron is constrained by symmetry to rotate around the threefold axis. Thus, the tilt angle is equal to $[180 - \angle(BOB)]/2$ and would be the primary order parameter for a pure tilt transition. The square of the tilt angle shows an approximate linear variation with pressure (see Fig. 6 and Table 4), similar to $LaAlO_3$ and $PrAlO_3$ $R\bar{3}c$ perovskites at high pressures

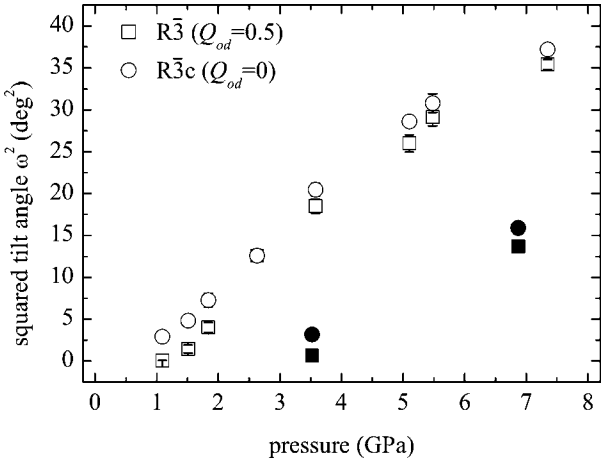

Figure 6
Pressure dependence of the squared tilt angle ω^2 for $R\bar{3}$ and $R\bar{3}c$ refinements. PST and PST-Ba are represented by open and filled symbols, respectively.

Table 4
Structural parameters for PST and PST-Ba obtained from refinements to neutron powder diffraction data in $R\bar{3}c$.

Parameters in square brackets are for constrained $R\bar{3}$ refinements.

P (GPa)	U^{11} (100 × Å^2)	U^{33} (100 × Å^2)	U^{eq} (100 × Å^2)	x	$\angle(B-O-B)$ (°)	$\omega(p)$ (°)	$\omega^2(p)$ (°)
PST							
1.09 (2)	3.8 (5) [4.0 (10)]	4.8 (12) [4.6 (19)]	4.2 (5) [4.2 (9)]	0.5104 (9) [0.5015 (24)]	176.6 (3) [179.5 (0)]	1.7 (2) [0.2 (0)]	2.9 (5) [0.1 (0)]
1.51 (2)	2.8 (3) [2.6 (3)]	6.0 (6) [6.4 (6)]	3.9 (3) [3.9 (3)]	0.5137 (8) [0.5073 (13)]	175.6 (3) [177.6 (4)]	2.2 (2) [1.2 (2)]	4.8 (7) [1.4 (5)]
1.84 (3)	2.7 (2) [2.4 (2)]	5.4 (6) [6.0 (6)]	3.6 (2) [3.6 (2)]	0.5167 (7) [0.5124 (9)]	174.6 (3) [176.0 (3)]	2.7 (2) [2.0 (1)]	7.3 (8) [4.0 (6)]
2.63 (3)	1.8 (2) [1.8 (2)]	6.1 (5) [6.1 (5)]	3.2 (2) [3.2 (2)]	0.5205 (5) [0.5199 (6)]	172.9 (2) [172.9 (2)]	3.5 (1) [3.5 (1)]	12.6 (7) [12.6 (7)]
3.58 (3)	1.5 (2) [1.5 (2)]	5.3 (5) [5.4 (5)]	2.8 (2) [2.8 (2)]	0.5280 (4) [0.5267 (5)]	170.9 (2) [171.4 (2)]	4.5 (1) [4.3 (1)]	20.5 (8) [18.5 (9)]
5.10 (4)	1.1 (1) [1.0 (1)]	5.1 (4) [5.3 (4)]	2.4 (2) [2.4 (2)]	0.5331 (4) [0.5316 (4)]	169.3 (1) [169.8 (2)]	5.3 (1) [5.1 (1)]	28.6 (7) [26.0 (10)]
5.48 (5)	1.5 (2) [1.4 (2)]	4.2 (5) [3.8 (5)]	2.4 (2) [2.2 (2)]	0.5342 (5) [0.5333 (6)]	168.8 (2) [169.2 (2)]	5.5 (1) [5.4 (1)]	30.8 (11) [29.2 (11)]
7.35 (4)	1.5 (9) [1.5 (9)]	3.3 (3) [3.1 (3)]	2.1 (6) [2.1 (6)]	0.5377 (3) [0.5365 (3)]	167.7 (1) [168.1 (1)]	6.1 (1) [6.0 (1)]	37.2 (6) [35.4 (6)]
BaPST							
3.52 (3)	1.2 (1) [1.2 (1)]	8.0 (4) [8.0 (4)]	3.5 (2) [2.2 (2)]	0.5110 (9) [0.5048 (22)]	176.4 (2) [178.4 (3)]	1.8 (2) [0.8 (4)]	3.2 (5) [0.6 (5)]
6.87 (4)	0.5 (1) [0.4 (1)]	7.1 (4) [7.2 (4)]	2.7 (2) [2.7 (1)]	0.5246 (5) [0.5229 (5)]	172.0 (2) [172.6 (2)]	4.0 (1) [3.7 (1)]	15.9 (7) [12.7 (6)]

(Zhao *et al.*, 2004, 2009), corresponding to second-order behaviour in terms of Landau theory.

An extrapolation to zero of the squared tilt angles measured at high pressures suggests that tilting may already occur at 1.1 GPa (see Fig. 6), *i.e.* below the critical pressure of 1.9 GPa determined from the static elastic softening in single-crystal XRD measurements (Mihailova, Angel *et al.*, 2008). This is supported by the result that refinements show a significantly non-zero tilt angle at 1.5 and 1.1 GPa, even though there is no significant intensity detected at the ooo peak positions. It therefore appears that, on increasing pressure, the structure may first develop a rhombohedral pattern of tilts within a unit cell that maintains a global cubic metric and then subsequently undergoes a macroscopic transition to a phase with a distorted (non-cubic) unit cell.

In order to determine whether the results of the refinement in $R\bar{3}c$ symmetry, and in particular the magnitudes of the octahedral tilts, are being biased by the setting of $Q_{od} = 0$ (complete B-site disorder), we also performed refinements in $R\bar{3}$ symmetry, which allows B-site ordering as well as other rotations and distortions of the octahedron due to the general position of the oxygen (Megaw & Darlington, 1975). In this space group the B and Pb cations can also be displaced along the threefold axis. However, general refinements were unstable which is consistent with the symmetry restriction of the distortion having a c-glide, as discussed above. Therefore, we constrained the refinements to match $R\bar{3}c$ symmetry except for the B-site cation ordering. A free refinement of Q_{od} results in $Q_{od} = 0$, corresponding to the $R\bar{3}c$ model. Thus, for the purpose of testing, Q_{od} was fixed to 0.5, which means site occupancies of 0.25/0.75 for the B cations, thus greatly overestimating the known contribution of the B-site order to the intensities of the ooo reflections. However, comparison of the refinements in $R\bar{3}c$ and constrained $R\bar{3}$ at high pressures (Table 2) shows that the refined $\omega^2(p)$ is not strongly dependent upon the value chosen for Q_{od} (Fig. 6). Close to the transition, however, the tilt angle is smaller for the refinement with $Q_{od} = 0.5$, as expected. Note that for most datasets, the $R\bar{3}c$ refinement with $Q_{od} = 0$ produces a slightly better statistical fit to the data. The atomic displacement parameters for the atoms in the $R\bar{3}c$ and the $R\bar{3}$ ($Q_{od} = 0.5$) refinements are very similar. There is no significant change in the isotropic displacement parameter of the B cation in either refinement with pressure. The range of values is 0.005–0.007 Å^2, corresponding to mean displacements of 0.08 Å.

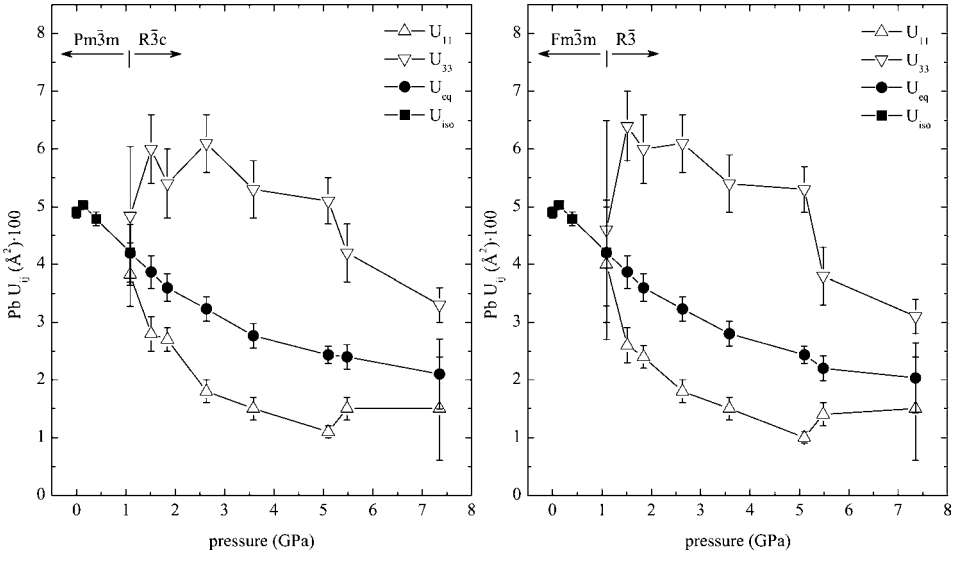

Figure 7
Pressure dependence of the isotropic and anisotropic Pb atomic displacement parameters of PST obtained by refinements to neutron powder diffraction data in $Pm\bar{3}m$/$Fm\bar{3}m$ at low pressures and in $R\bar{3}c$/$R\bar{3}$ at high pressures. The chemically B-site ordered structures were refined with a $Q_{od} = 0.5$ and exhibit the same results as the disordered structures within the uncertainties.

The evolution of the equivalent isotropic displacement parameter for the Pb cation at higher pressures is entirely continuous with the values refined for the isotropic displacement parameter in the

cubic phase at lower pressures (Fig. 7). Both refinements in $R\bar{3}c$ and $R\bar{3}$ show the Pb cation to be isotropic at 1.09 (2) GPa with a mean displacement of 0.2 Å. At 1.5 GPa the Pb cation becomes significantly anisotropic, with $U^{33} > U^{11}$ (Fig. 7 and Table 4) corresponding to larger displacements along the cubic ⟨111⟩ direction. The value of 0.06 Å^2 for U^{33} corresponds to mean displacements of 0.24 Å. With increasing pressure both the displacements and the anisotropy decreases. If the trends were extrapolated to higher pressures, the Pb would become isotropic again around 10–12 GPa, with $U_{iso} \sim 0.015$ Å^2, and mean displacement of 0.12 Å. The Pb cations are at the special positions $00z$ and $00z + \frac{1}{2}$, lying on the *c*-glide plane in the rhombohedral space groups. Therefore, as mentioned above, Pb shifts can only contribute to reflections with $l = 2n$, indexed in $Fm\bar{3}m$, which remain $l = 2n$ reflections in $R\bar{3}c$, and cannot be responsible for the increasing intensity of the $l = 2n + 1$ reflections in the high-pressure phase. It should be emphasized that the Pb position always refined to $00\frac{1}{4}$, indicating that there are, on average, no off-centre displacements of the Pb cations with respect to their position in the prototype cubic structure. Thus, there is no evidence for the long-range order of Pb off-centre displacements and the refined anisotropy must therefore be attributed to Pb displacements along the cubic ⟨111⟩ direction that are, at most, ordered on a local length scale.

Refinements of the high-pressure structure to the single-crystal XRD data are complicated by the twinning that must be present within the single-crystal sample as a result of the phase transition to rhombohedral symmetry. The refinements of the structure were therefore performed with a structure model in a unit-cell with a cubic metric, an *F*-lattice, an inversion centre at the origin, and a single threefold axis parallel to [111]. The twinning was then modelled as a four-component twin generated by a fourfold rotation around [001], corresponding to the symmetry lost on transformation from cubic to rhombohedral symmetry. Due to a combination of the relatively weak scattering from the O atoms and the twinning, it is not possible to refine the oxygen positional parameter. Thus, it was fixed to a value interpolated from the refinements to neutron powder diffraction data. The occupancies of the *B* sites were fixed to the values determined at 0.5 GPa, corresponding to $Q_{od} = 0.08$. The Pb cation was fixed at $\frac{1}{4}\frac{1}{4}\frac{1}{4}$. Together these restraints correspond to $R\bar{3}c$ symmetry, apart from the chemical *B*-site cation ordering. The resulting refinements show that the anisotropy of Pb has the same sense as for the refinements to the neutron data, but the degree of anisotropy is smaller, and the overall decrease in U^{ij} with pressure is not as great (Fig. 8). The 1.7 GPa X-ray dataset does not indicate anisotropic Pb, whereas the neutron powder dataset at 1.5 GPa does, which may be the reason for the small jump from U_{iso} in the space group $Fm\bar{3}m$ to the U_{eq} in the space group $R\bar{3}$. These differences may be in part due to using an empirical extinction model in *SHELX* for the X-ray refinements.

3.2.2. Tetragonal and orthorhombic systems. The symmetry of the structural distortion, restricted to having a glide symmetry along ⟨111⟩ cubic, is not limited to the rhombohedral space group $R\bar{3}c$. The tilt systems $a^0a^0c^-$ (*I*4/*mcm*) and $a^0b^-b^-$ (*Imma*) are also allowed by the appearance of the additional ooo reflections without violating the glide symmetry.

Refinements in *I*4/*mcm* ($a^0a^0c^-$) with complete *B*-site disorder consistently give significantly worse fits to the neutron powder diffraction data than the corresponding refinement in $R\bar{3}c$ ($a^-a^-a^-$). Thus, *I*4/*mcm* can be excluded as a possible space-group candidate. This is presumably because *I*4/*mcm* has tilts only about one of the ⟨001⟩ axes of the cubic aristotype, whereas $R\bar{3}c$ has the octahedra tilted about [111] of the cubic structure, which is equivalent to equal tilts about the three cubic axes [100], [010] and [001]. However, the space

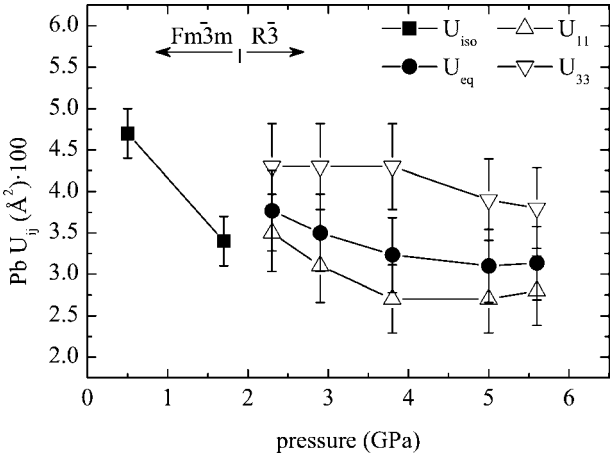

Figure 8
Pressure dependence of the Pb atomic displacement parameters of PST obtained by refinements to synchrotron single-crystal XRD data.

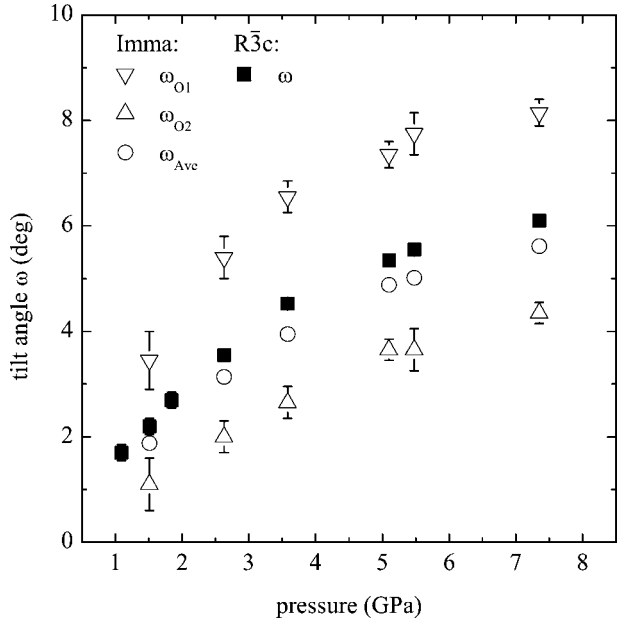

Figure 9
Pressure dependence of the two tilt angles in space group *Imma*, corresponding to the two types of O atoms. The average tilt angle is compared to the tilt angle in the space group $R\bar{3}c$.

group *Imma* allows equal tilts about two of these three cubic axes, corresponding to rotation around [110] cubic, with the tilt system $a^0b^-b^-$ in a unit cell of $(2)^{1/2}a$ by $2a$ by $(2)^{1/2}a$ (for $a \simeq 4$ Å). Refinements in *Imma* have a quality of fit indistinguishable from that of the $R\bar{3}c$ model, although they require considerable damping to keep them stable. The O site is split to O_1 at $0\frac{1}{4}z$, $z \simeq 0.25$, and O_2 at $x00$, $x \simeq \frac{1}{4}$ (Woodward, 1997). The displacement parameters of the O atoms in *Imma* are unusually large, but the positional parameters provide trends in the two *Imma* tilt angles that parallel those for the rhombohedral refinements, with the average tilt following the $R\bar{3}c$ values closely (Fig. 9). The tilt angles are also clearly non-zero below 1.51 (2) GPa. Thus, *Imma* cannot be excluded as a possible model for the high-pressure phase of PST.

The *B*-cation site is constrained to lie on an inversion centre in *Imma*, but the Pb site becomes a special position at $0\frac{1}{4}z$, with $z \simeq 0.75$, which allows the Pb cations to be displaced in an anti-ferroic pattern parallel to [001] of the orthorhombic unit cell, corresponding to ⟨110⟩ of the cubic unit cell. However, as we already have shown, there is no requirement for the Pb to be shifted, thus the Pb position always refines back to $z = \frac{3}{4}$ in both isotropic and anisotropic refinements. In contrast to $R\bar{3}c$, the Pb has $U^{22} \simeq 2.5U^{11} \sim 4U^{33}$ (Fig. 10), which suggests large displacements along the ⟨110⟩ cubic directions. Nonetheless, they show the same general behaviour as those obtained from the $R\bar{3}c$ and constrained $R\bar{3}$ refinements (Fig. 10).

However, there are a few features that suggest that the *Imma* model is a worse representation of the structure than $R\bar{3}c$. As mentioned above, the refinements in *Imma* require considerable damping to keep them stable and the additional parameters do not improve the reduced χ^2 values compared with the refinements in $R\bar{3}c$. In addition, there is a discontinuity from the U_{iso} refined in $Pm\bar{3}m$ to the U_{eq} of *Imma* (see Fig. 10). Finally, the phase transition from $Pm\bar{3}m$ to *Imma* (or for *B*-site ordered structures $Fm\bar{3}m$ to $C2/m$) is required to be of first order by Landau theory (Howard *et al.*, 2003; Howard & Stokes, 2005), whereas the evolution of both the structure and the unit-cell parameters (Mihailova, Angel *et al.*, 2008) indicate that the observed phase transition near 1.9 GPa is second order in character.

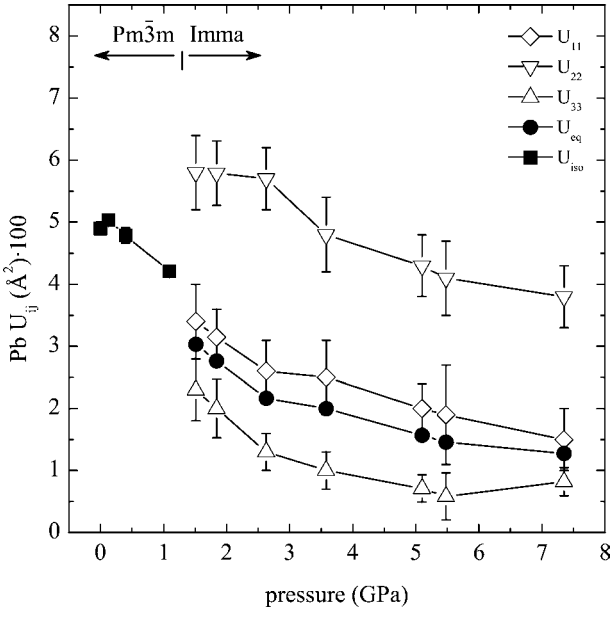

Figure 10
Pressure dependence of the isotropic and anisotropic Pb atomic displacement parameters of PST obtained by refinements to neutron powder diffraction data in $Pm\bar{3}m$ at low pressures and in *Imma* at high pressures.

3.3. High-pressure phase: PST-Ba

Following the results for PST, refinements were based upon a $R\bar{3}c$ model (Table 3). Again, a $R\bar{3}$ model constrained to $R\bar{3}c$ was used to determine the influence of chemical *B*-site cation ordering, giving the same results as for the $R\bar{3}c$ model within the uncertainties. Only the octahedral tilt angle $\omega(p)$ has slightly smaller values as expected. The extrapolation of the squared tilt angle data suggests the appearance of long-range ordering of tilts near 3 GPa (see Fig. 6). Fig. 11 shows the refined Pb displacement parameters. The U_{iso} decreases with increasing pressure as in PST, however, in contrast to PST, the anisotropy is larger in the high-pressure phase (Table 4). This can be the result of two features: the *B*-site ordered regions are larger in PST-Ba, allowing the Pb to shift the most along the cubic ⟨111⟩ direction, corresponding to the U^{33} displacement parameter; and the incorporation of Ba^{2+} having an isotropic electron shell destroys the coupling of the stereochemically active Pb^{2+} cations along the cubic ⟨110⟩ direction (Mihailova, Maier *et al.*, 2008), which reduces the corresponding $U^{11} = U^{22}$ displacement parameters. This is

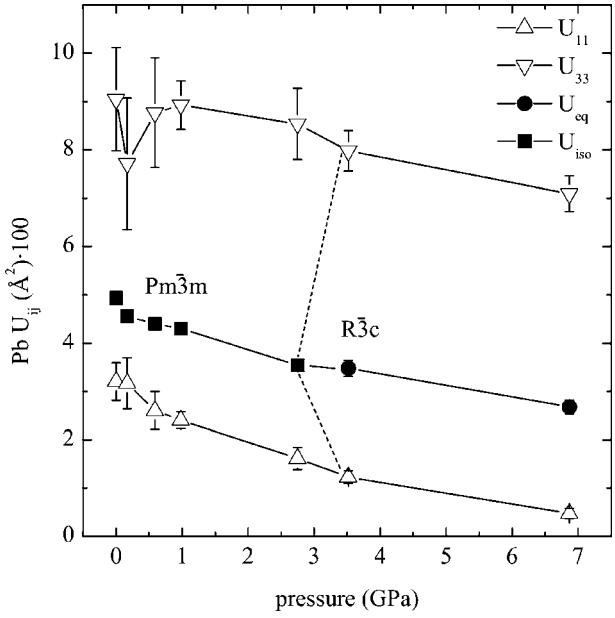

Figure 11
Pressure dependence of the isotropic and anisotropic Pb displacement parameters of PST-Ba refined in $Pm\bar{3}m$ at low pressures and $R\bar{3}c$ at low and high pressures. Below 3.52 GPa, the structure refines significantly better in $Fm\bar{3}m$. However, in contrast to pure PST, the anisotropic displacement of the Pb cations persists down to ambient pressure due to elastic barriers induced by Ba doping.

supported by the result that a rhombohedral refinement below 3.53 (3) GPa does not lead to isotropic Pb displacement values but rather shows the persistence of the anisotropy down to ambient pressure (Fig. 11).

For completeness, refinements of the PST-Ba data were also performed with $I4/mcm$ and *Imma* models. The $I4/mcm$ model gave significantly worse fits to the data as it did for pure PST. The *Imma* model resulted in negative U^{22} displacement parameters for the O atoms, thus giving another strong indication that the rhombohedral symmetry is the most plausible for the high-pressure phase of Pb-based perovskite-type relaxors.

Finally, we note that all of the peaks (both ooo and eee) in the neutron powder diffraction datasets from both PST and PST-Ba display broadening at the highest pressures, above 5 GPa for PST, and at 6.9 GPa for PST-Ba. The Rietveld refinements show that this increase in width occurs for both the Gaussian and Lorentzian components of the pseudo-Voigt functions used to model the peak shapes. For PST at 7.35 (4) GPa, both refined width parameters are approximately twice the values of the instrumental resolution, whereas for PST-Ba at 6.87 (4) GPa, they increased by approximately one-third. The uniformity of broadening of all peaks, and the fact that it is the same whatever symmetry is chosen for the structure model suggest that it is not due to a further symmetry reduction. Exploration of various refinement models for the broadening suggests that it arises from isotropic strain.

4. Discussion and conclusions

Previous XRD experiments on PST revealed an elastic phase transition occurring near 1.9 GPa (Mihailova, Angel *et al.*, 2008). The new neutron powder and synchrotron single-crystal X-ray data show that the transition is associated with a structural evolution that results in a continuous and significant increase in the intensities of ooo reflections, with the exception of the 111 reflection (as indexed in space group $Fm\bar{3}m$). The constancy of the 111 reflection is critical; it shows that the structural distortion arising from the phase transition must have a glide pseudo-symmetry along the ⟨111⟩ cubic directions and, because the Pb cations occupy special positions, it means that they cannot contribute to the intensities of the ooo reflections. Since the degree of *B*-site cation ordering is unlikely to change with pressure at room temperature, these arguments are alone sufficient to demonstrate that the structural evolution of PST above the phase transition must involve octahedral tilting.

No other classes of reflections appear in either the X-ray or neutron diffraction patterns, which unambiguously identifies the octahedral tilting pattern as being anti-phase in character. Refinements to the neutron powder diffraction data in the three possible space groups with the highest symmetry, namely $R\bar{3}c$ ($a^-a^-a^-$), $I4/mcm$ ($a^0a^0c^-$) and *Imma* ($a^0b^-b^-$), corresponding to complete *B*-site disorder, all confirm that octahedral tilting explains the evolution of the diffraction patterns. It is found that $R\bar{3}c$ and *Imma* provide significantly better fits to the data than $I4/mcm$, and that the $R\bar{3}c$ refinement results are more physically reasonable. This strongly suggests that the tilt system involves simultaneous anti-phase tilts around all three pseudo-cubic axes. Refinements in $R\bar{3}$ of a model with an unrealistically large degree of *B*-site cation order also confirm the development of octahedral tilting.

In discussing the refined structures it is crucial to bear in mind that they constitute some form of time and space average over a complex local nanoscale structure that, at least at ambient conditions, is comprised of dynamic polar nanoregions overlain upon spatial regions exhibiting either chemical *B*-site cation order or disorder. The average structure that is obtained from refinement to Bragg diffraction intensities therefore depends not only on the types of local domains present in the sample, but also on their sizes, relative orientations and characteristic atomic displacements. Thus, the refined structure represents the long-range order present in the sample, but the long-range order parameter determined in this way will almost always be much smaller than the short-range order present on the local scale of a few unit cells.

With these considerations in mind we can now interpret the results of the structure refinements to the X-ray and neutron diffraction data. In the case of PST, from ambient pressure to 1.1 GPa, the Pb cations are locally displaced but are not ordered on the diffraction length scale. If octahedral tilts are present, then they are only coherent over a short length scale, and the metric of the structure remains cubic. The isotropic atomic displacement parameter of Pb initially decreases with increasing pressure, as would be expected. However, at 1.5 GPa the displacement ellipsoids become significantly anisotropic, elongated along the cubic ⟨111⟩ directions. Structural refinements revealed no evidence for coherent static displacements of Pb cations, which indicates that they can only be locally ordered. Although the presence of glide symmetry in the global structure requires anti-ferroic Pb displacements, locally they could be ferroically ordered. The development of the Pb displacement anisotropy is associated with the development of anti-phase tilting of the BO_6 octahedra, but within a unit-cell metric that initially remains cubic. The octahedral tilting develops continuously with increasing pressure, leading to an average symmetry decrease from cubic to rhombohedral. The weak diffuse scattering streaks along ⟨100⟩* associated with the ooo peaks indicate that the tilting is not completely homogenous across the entire single crystal, and that there are faults or domain walls parallel to {100} cubic. Whether the streaks are solely the result of the development of rhombohedral domains all of which have the same degree of tilt but of different orientations, or also arise from domains with different degrees of octahedral tilts, cannot be determined from the available data. We attribute the broadening of the reflections at higher pressures to the development of coherency strains which become larger as the rhombohedral distortion from cubic increases; that is the regions close to the domain walls will be strained to coherently match the neighbouring domains, while the interiors of the domains will relax and exhibit the full rhombohedral distortion.

The heavily Ba-doped compound shows the same development of structural distortion, but shifted to higher pressures. This can be understood as the result of two effects. The substitution of the larger Ba cation for Pb introduces elastic fields that expand the structure and thus delay the development of octahedral tilting. Further, the Ba dilutes the Pb, thus reducing the coherency in the PbO system (Welsch, Maier *et al.*, 2009) and the cooperative development of local displacements of the Pb cations. Together, the results on pure PST and PST-Ba therefore suggest that the transition to the high-pressure phase is initially a cooperative phenomenon involving both the development of short-range ordering of Pb displacements along ⟨111⟩ cubic and octahedral tilting. Higher pressures drive further octahedral tilting (as the mechanism to reduce the volume; Angel *et al.*, 2005) and this consequently reduces the *A*-site cavity volume and hence the overall magnitude of Pb displacements. Based on the high-pressure data published on PMN (Chaabane *et al.*, 2003; Rotaru *et al.*, 2008), PZN (Janolin *et al.*, 2006), PMT (Gvasaliya *et al.*, 2006) and PSN (Maier *et al.*, 2010) we propose that the same pattern of long-range-ordered anti-phase octahedral tilts and short-range ordered Pb displacements also develops in these compounds at high pressures, and is therefore a common feature of the high-pressure phases of lead-based perovskite-type relaxor ferroelectrics.

Experiments at the ISIS Pulsed Neutron and Muon Source were supported by a beamtime allocation from the Science and Technology Facilities Council and the EU funded NMI3 programme. Financial support by the Deutsche Forschungsgemeinschaft (MI 1127/2 and GK 611), the National Science Foundation (EAR-0738692), and the Bulgarian Ministry of Science and Education (BY-X-308) is gratefully acknowledged. We would like to thank Duncan Francis from the ISIS support staff for providing technical assistance during the experiments.

References

Ahart, M., Cohen, R. E., Struzhkin, V., Gregoryanz, E., Rytz, D., Prosandeev, S. A., Mao, H.-K. & Hemley, R. J. (2005). *Phys. Rev. B*, **71**, 144102.
Angel, R. J., Bujak, M., Zhao, J., Gatta, G. D. & Jacobsen, S. D. (2007). *J. Appl. Cryst.* **40**, 26–32.
Angel, R. J., Zhao, J. & Ross, N. L. (2005). *Phys. Rev. Lett.* **95**, 025503.
Baba-Kishi, K. Z., Cressey, G. & Cernik, R. J. (1992). *J. Appl. Cryst.* **25**, 477–487.
Besson, J. M., Nelmes, R. J., Hamel, G., Loveday, J. S., Weill, G. & Hull, S. (1992). *Physica B*, **180**, 907–910.
Bhalla, A. S., Guo, R. & Roy, R. (2000). *Mater. Res. Innovations*, **4**, 3–29.
Blinc, R., Gregorovi, A., Zalar, B., Pirc, R. & Lushnikov, S. G. (2000). *Phys. Rev. B*, **61**, 253.
Boehler, R. (2006). *Rev. Sci. Instrum.* **77**, 115103.
Bokov, A. A. & Ye, Z.-G. (2006). *J. Mater. Sci.* **41**, 31–52.
Bursill, L. A., JuLin, P., Hua, Q. & Setter, N. (1995). *Physica B*, **205**, 305–326.
Burton, B. P., Cockayne, E. & Waghmare, U. V. (2005). *Phys. Rev. B*, **72**, 064113.
Chaabane, B., Kreisel, J., Bouvier, P., Lucazeau, G. & Dkhil, B. (2004). *Phys. Rev. B*, **70**, 134114.
Chaabane, B., Kreisel, J., Dkhil, B., Bouvier, P. & Mezouar, M. (2003). *Phys. Rev. Lett.* **90**, 257601.
Glazer, A. M. (1972). *Acta Cryst.* B**28**, 3384–3392.
Goodwin, A. L., Redfern, S. A. T., Dove, M. T., Keen, D. A. & Tucker, M. G. (2007). *Phys. Rev. B*, **76**, 174114.
Gruverman, A. & Kholkin, A. (2006). *Rep. Prog. Phys.* **69**, 2443–2474.
Gvasaliya, S. N., Pomjakushin, V., Roessli, B., Strässle, T., Klotz, S. & Lushnikov, S. G. (2006). *Phys. Rev. B*, **73**, 212102.
Hirota, K., Wakimoto, S. & Cox, D. E. (2006). *J. Phys. Soc. Jpn*, **75**, 111006.
Howard, C. J., Kennedy, B. J. & Woodward, P. M. (2003). *Acta Cryst.* B**59,** 463–471.
Howard, C. J. & Stokes, H. T. (2005). *Acta Cryst.* A**61**, 93–111.
ISIS Annual Report (1996). Rutherford Appleton Laboratory Report, RAL-TR-96-050, 61–62.
ISIS Annual Report (1997). Rutherford Appleton Laboratory Report, RAL-TR-97-050, 28–29.
Janolin, P. E., Dkhil, B., Bouvier, P., Kreisel, J. & Thomas, P. A. (2006). *Phys. Rev. B*, **73**, 094128.
Kleemann, W., Dec, J. & Westwański, B. (1998). *Phys. Rev. B*, **58**, 8985–8990.
Kreisel, J., Bouvier, P., Dkhil, B., Thomas, P. A., Glazer, A. M., Welberry, T. R., Chaabane, B. & Mezouar, M. (2003). *Phys. Rev. B*, **68**, 014113.
Kreisel, J., Dkhil, B., Bouvier, P. & Kiat, J. M. (2002). *Phys. Rev. B*, **65**, 172101.
Larson, A. C. & Von Dreele, R. B. (1994). *GSAS*, Report LAUR 86–748. Los Alamos National Laboratory, New Mexico, USA.
Maier, B. J., Welsch, A.-M., Angel, R. J., Mihailova, B., Zhao, J., Engel, J. M., Schmitt, L. A., Paulmann, C., Gospodinov, M., Friedrich, A. & Bismayer, U. (2010). *Phys. Rev. B*. In the press.
Marinova, V., Mihailova, B., Malcherek, T., Paulmann, C., Kovacs, K. L. L., Veleva, M., Gospodinov, M., Güttler, B. & Bismayer, R. S. U. (2006). *J. Phys. Condens. Matter*, **18**, L385–L393.
Marinova, V., Petrova, D., Gospodinov, M. & Dobreva, S. (1997). *Mater. Res. Bull.* **32**, 663.
Marshall, W. G. & Francis, D. J. (2002). *J. Appl. Cryst.* **35**, 122–125.
Megaw, H. D. & Darlington, C. N. W. (1975). *Acta Cryst.* A**31**, 161–173.
Mihailova, B., Angel, R. J., Welsch, A.-M., Zhao, J., Engel, J., Paulmann, C., Gospodinov, M., Ahsbahs, H., Stosch, R., Güttler, B. & Bismayer, U. (2008). *Phys. Rev. Lett.* **101**, 017602.
Mihailova, B., Maier, B., Paulmann, C., Malcherek, T., Ihringer, J., Gospodinov, M., Stosch, R., Güttler, B. & Bismayer, U. (2008). *Phys. Rev. B*, **77**, 174106.
Munro, R. G., Piermarini, G. J., Block, S. & Holzapfel, W. B. (1985). *J. Appl. Phys.* **57**, 165–169.
Nelmes, R. J., Loveday, J. S., Wilson, R. M., Besson, J. M., Klotz, S., Hamel, G. & Hull, S. (1994). *Proceedings of the Symposium on Time-of-Flight Diffraction at Pulsed Neutron Sources*, Vol. 29, pp. 19–27. American Crystallographic Association, Buffalo, New York.
Oxford Diffraction (2007). *CrysAlis*. Oxford Diffraction Ltd, Abingdon, Oxfordshire, England.
Paulmann, C. & Malcherek, T. (2006). HASYLAB Annual Report, Part I, pp. 1399–1400.
Peng, J. L. & Bursill, L. A. (1993). *Mod. Phys. Lett. B*, **7**, 609–621.
Rotaru, G.-M., Gvasaliya, S. N., Pomjakushin, V., Roessli, B., Strässle, T., Lushnikov, S. G., Shaplygina, T. & Günter, P. (2008). *J. Phys. Condens. Matter*, **20**, 104235.
Samara, G. A. (2003). *J. Phys. Condens. Matter*, **15**, R367–R411.
Sheldrick, G. M. (2008). *Acta Cryst.* A**64**, 112–122.
Takesue, N., Fujii, Y., Ichihara, M. & Chen, H. (1999). *Phys. Rev. Lett.* **82**, 3709–3712.
Tkachuk, A. & Chen, H. (2003). Personal communication, http://www.citebase.org/abstract?id=oai%3AarXiv.org%3Acond-mat%2F0303012.

Toby, B. H. (2001). *J. Appl. Cryst.* **34**, 210–213.
Welsch, A.-M., Maier, B. J., Engel, J., Mihailova, B., Angel, R. J., Paulmann, C., Gospodinov, M., Friedrich, A., Stosch, R., Güttler, B. & Bismayer, U. (2009). *Phys. Rev. B*, **80**, 104118.
Welsch, A.-M., Mihailova, B., Gospodinov, M., Stosch, R., Güttler, B. & Bismayer, U. (2009). *J. Phys. Condens. Matter*, **21**, 235901.
Woodward, P. M. (1997). *Acta Cryst.* B**53**, 32–43.
Zhao, J., Ross, N. L. & Angel, R. J. (2004). *J. Phys. Condens. Matter*, **16**, 8763–8773.
Zhao, J., Ross, N. L., Angel, R. J., Carpenter, M. A., Howard, C. J., Pawlak, D. A. & Lukasiewicz, T. (2009). *J. Phys. Condens. Matter*, **21**, 235403.
Zhou, D. H., Hoatson, G. L., Vold, R. L. & Fayon, F. (2004). *Phys. Rev. B*, **69**, 134104.